Friction, adhesion, and elasticity of graphene edges

D. Patrick Hunley, Tyler J. Flynn, Tom Dodson, Abhishek Sundararajan, Mathias J. Boland, and Douglas R. Strachan

Phys. Rev. B **87**, 035417 — Published 22 January 2013

DOI: 10.1103/PhysRevB.87.035417

Friction, Adhesion, and Elasticity of Graphene Edges

D. Patrick Hunley, Tyler J. Flynn, Tom Dodson, Abhishek Sundararajan, Mathias J. Boland, and Douglas R. Strachan*

University of Kentucky, Department of Physics & Astronomy, Lexington, KY 40506

Corresponding Author* **(**Email: doug.strachan@uky.edu)

RECEIPT DATE (August 27, 2012)

ABSTRACT:

Frictional, adhesive, and elastic characteristics of graphene edges are determined through lateral force microscopy. Measurements reveal a significant local frictional increase at exposed graphene edges, whereas a single overlapping layer of graphene removes this local frictional increase. Comparison of lateral force and atomic force microscopy measurements shows that local forces on the probe are successfully modeled with a vertical adhesion in the vicinity of the atomic-scale graphene steps which also provides a new low-load calibration method. Lateral force microscopy performed with carefully maintained low-adhesion probes shows evidence of elastic straining of graphene edges. Estimates of the energy stored of this observed elastic response is consistent with out-of-plane bending of the graphene edge.

PACS (81.05.ue, 81.07.Lk, 46.55.+d, 62.25.-g, 68.35.Af, 62.20.de)

I. INTRODUCTION

Graphene has tremendous potential for use in a wide range of applications owing to its incredible mechanical, thermal, and electronic properties.[1-4] The structural properties of graphene edges are expected to play an important role in electrical and thermal transport,[5, 6] particularly as the dimensions of graphene elements are reduced to the nanoscale.[7-10] In addition, strain within graphene can induce an effective local magnetic field[11-15] making recently proposed strain effects in the vicinity of graphene edges particularly important in determining transport properties of graphene nanostructures,[11, 16-19] while recent theoretical work has also raised the possibility that strain along the graphene edge could inhibit quantum Hall effect physics.[17, 20] Although recent investigations of the mechanical properties of bulk graphene have demonstrated its tremendous strength[21] and low friction,[22-25] such characteristics have been relatively unexplored in the vicinity of its edges.

Lateral force microscopy (LFM), which is the measurement of torsional deflections of a cantilever as it is dragged over a surface, has been used over the last few decades to probe nanometer-scale frictional and topographic features.[26] Although it has long been known that there are significant increases in lateral force signals at atomic scale steps,[27, 28] the source of these increases has been of ongoing debate.[24, 29-31] Elimination of these localized increases, while maintaining the overall atomic-scale surface topography, could have significant implications towards the realization of low-friction micro- and nano-electromechanical systems.

Here we report on frictional, adhesive, and elastic characteristics of graphene edges through the use of lateral force microscopy. LFM reveals a significant local frictional increase at the exposed edges of graphene, whereas a single overlapping layer of graphene nearly completely

removes this local frictional increase. This result indicates graphene could be an ideal, atomically thin coating for reducing local friction associated with atomic steps. Direct comparison between LFM and atomic force microscopy (AFM) measurements shows that the local forces on the scanning probe are successfully modeled with a vertical adhesion in the vicinity of the atomic-scale graphene steps. Taking this adhesion into account allows for the surface topography of graphene to be determined through low-load LFM measurements and also provides a new low-load LFM calibration method. Through the use of carefully maintained scanning probe tips, we also observe evidence of elastic straining of graphene edges, which behave as nanoscale springs. Estimates of the strain energy are consistent with out-of-plane bending of graphene edges when sharp LFM tips are dragged into them. The elastic response we observe represents the reversible straining of graphene edges and could represent a possible route for reversibly tuning the electronic properties of graphene.

II. METHODS

A. Sample preparation

The graphene samples were prepared through mechanical exfoliation of kish graphite onto silicon substrates with a 300 nm oxide layer.[2] Prior to exfoliation, the substrates were placed in an ultrasonic cleaner in acetone, isopropyl alcohol, and deionized water for 3 minutes each. This was followed by UV-ozone cleaning. After exfoliation, few-layer graphene films were initially identified through optical microscopy. The number of atomic layers was then determined through both Raman spectroscopy and AFM height measurements. The graphene films did not undergo any further processing.

B. Lateral force and adhesion measurements

The LFM measurements were performed with an Asylum Research MFP-3D atomic force microscope in ambient laboratory conditions (at a temperature of 20 ± 3 C° and a relative humidity of 20 ± 3 %). We used PPP-LFMR probes, manufactured by Nanosensors, which have nominal values of 0.2 N/m and 23 kHz for the force constant and resonant frequency, respectively (details of this model are discussed below in *Appendix B*). As usual in LFM, the scan angle is selected such that the cantilever beam is perpendicular to the fast scanning direction. Light from an infrared laser is reflected off the back of the cantilever and onto a four-quadrant position sensitive detector (PSD) in order to monitor both lateral and vertical deflections of the probe. When the tip is scanned across the sample surface, lateral forces cause the cantilever to undergo torsional rotation. This deflects the laser spot in the horizontal direction at the PSD. Simultaneously, the vertical deflection is maintained through closed-loop feedback control which provides topographical information of the scanned region. In these experiments, we utilized probes which minimized crosstalk between the horizontal and vertical laser spot deflections.[32]

Measurement of the adhesion force is done by bringing the tip into contact with the sample surface then retracting it while monitoring the deflection voltage to determine the force required to snap the tip off the sample surface. Details of these adhesion measurements and their relation to scanning probe tip properties are discussed below in *Appendix A*. Overall, we find that differences in the tip-graphene and tip-SiO_2 adhesion forces are negligible. The net load F_{net} is defined as the sum of the vertical applied load L by the scanning probe cantilever and the adhesion force A between the tip and sample. Applying a negative load L is possible by first bringing the tip into contact with the sample surface then allowing the adhesion force to maintain contact when the negative load is applied.

III. RESULTS AND DISCUSSION

To investigate the mechanical and frictional characteristics of graphene edges we focus on graphene crosses where one graphene layer obliquely overlaps a second layer. Such crosses occasionally occur during the mechanical exfoliation processes and provide two different edges for comparison -- one exposed and the other covered by a layer of graphene. Figure 1a shows an atomic force microscopy (AFM) contact-mode height scan of a cross formed from two single layers of graphene that produced four distinct regions – two that are one atomic layer thick, a bilayer region, and the exposed SiO_2.

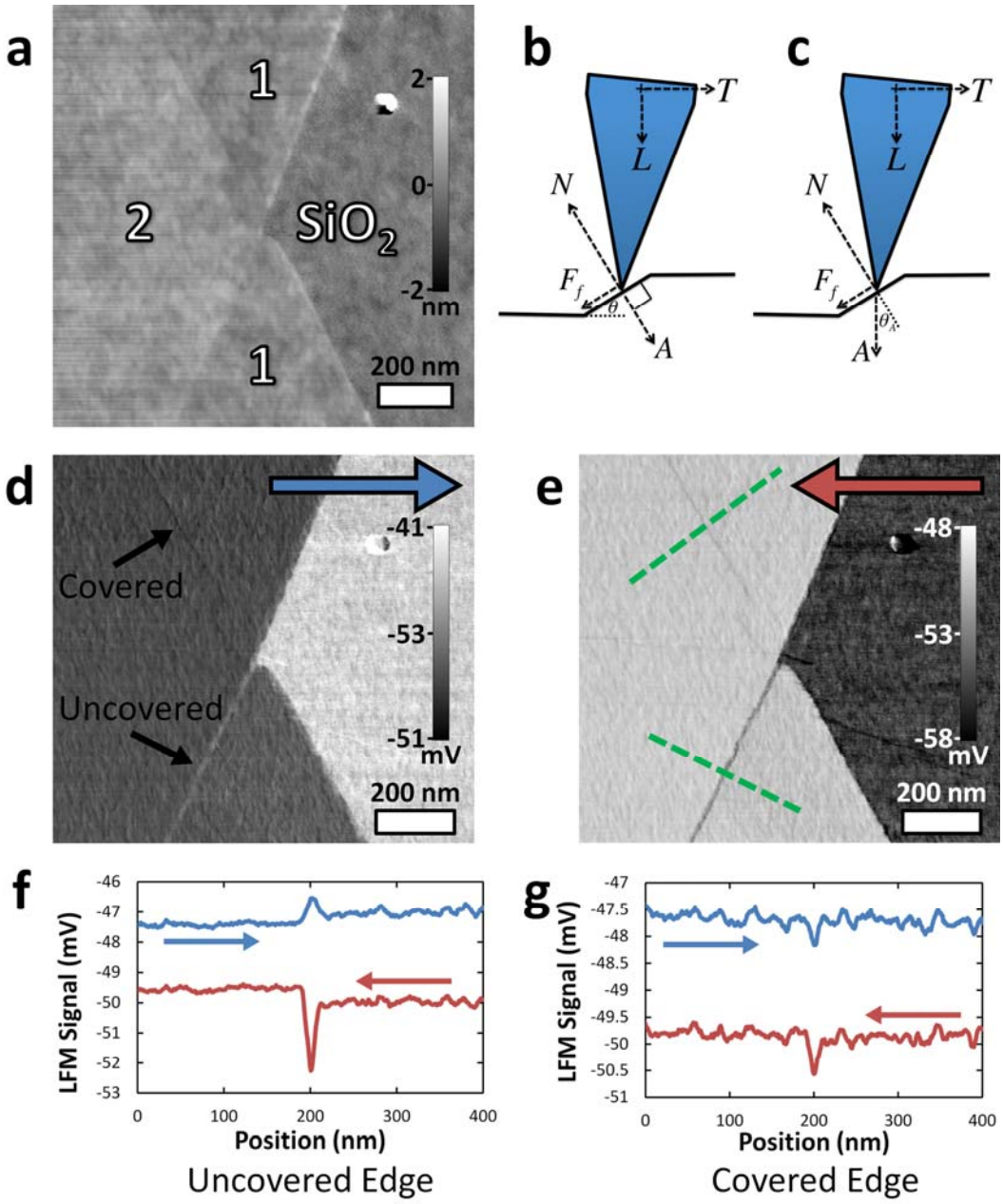

Figure 1: AFM and LFM of graphene crosses: **a,** Contact mode AFM height image of a graphene cross. **b-c,** Schematic diagram of LFM model with the adhesion directed normal (**b**) to the local surface and vertically (**c**) as the tip is dragged over a step. **d-e,** LFM scan image formed while scanning the tip in the "trace" direction (left to right) (**d**) and in the "retrace" direction (right to left) (**e**). **f-g,** Line scans taken from (**e**) along the green dashed lines for the uncovered (**f**) and covered (**g**) edges. Data represent the average of 150 adjacent line scans over a width of 146 nm. The data in **d-g** were taken with a net load F_{net} of 9.0 nN, where F_{net} is defined as the sum of the 6.7 nN load L applied by the cantilever tip and the 2.3 nN adhesion A of the tip to the surface determined through independent force plots.

Although the AFM height image of Fig. 1a does not show discernible differences between the boundaries, LFM (Figs. 1b and 1c) clearly distinguishes between the two types of edges. Figures 1d and 1e show the lateral signals simultaneously measured with the contact-mode data in Fig. 1a. Figure 1d corresponds to the "trace" image (scanning left to right) and Fig. 1e corresponds to the "retrace" image (scanning right to left). In both the trace and retrace LFM images, the uncovered edge has much greater contrast than the covered edge. Moreover, the uncovered edge shows both a positive and negative torsional deflection of the lateral probe depending on scan direction whereas the covered edge produces the same LFM deflection regardless of scan direction, clearly discernible in the line scans in Figs. 1f and 1g. These LFM measurements allow for the easy identification of covered or uncovered step edges, enabling one to determine the stacking arrangements and folds of few-layer graphene systems.

To quantify these results, we model the forces on an LFM tip as shown in Figs. 1b and 1c over a surface having a local incline angle θ (with details of this model discussed below in *Appendix B*). The forces on the tip are balanced by the forces and moments applied to the cantilever and will sum to zero assuming the tip is not accelerating. The forces applied to the cantilever are the transverse force T and the load force L while the resulting moment causes the torsional rotation of the cantilever. We model the tip sample interaction as a normal reaction force N and a frictional force obeying Amonton's law $F_f = \mu N$. In descriptions of interactions between macroscopic inclines and scanning probe tips,[33, 34] the adhesion A is typically modeled as an attractive force directed normal to the incline, as in Fig. 1b. However, this choice is not necessarily valid for very short inclines that occur for atomic scale changes in topography, so we allow A to have a variable direction ranging from the local surface normal (Fig. 1b) to the

vertical direction where $\theta = \theta_A$ (Fig. 1c). In the small angle approximation discussed in detail in *Appendix B*, the above model gives the local coefficient of friction,

$$\mu = \frac{\alpha \mathrm{W}_V}{(L+A)}, \tag{1}$$

which depends on the difference between trace and retrace LFM voltage measurements ($2\mathrm{W}_V = (V_t - V_r)$) and an LFM calibration coefficient α that converts the measured voltage to the lateral force on the cantilever tip. The model also gives the local incline assuming normal directed adhesion,

$$\theta = \frac{\alpha \Delta_{V_0}}{L+(L+A)\mu^2}, \tag{2}$$

while for vertical adhesion,

$$\theta = \frac{\alpha \Delta_{V_0}}{(L+A)(1+\mu^2)}. \tag{3}$$

These equations depend on the average of the trace and retrace voltage measurements ($\Delta_{V_0} = (V_t + V_r)/2 - V_0$) with a zero offset ($V_0$) estimated by averaging $(V_t + V_r)/2$ over a flat region.

Figures 2a and 2b show, respectively, LFM scans of an uncovered graphene edge and an edge covered by a single layer of graphene which (along with the LFM trace measurements not shown) is used to determine a spatially varying W_V and Δ_{V_0} and, thus, the local frictional variations and surface topography through Eqs. (1-3). Fig 2c is the coefficient of friction as a function of position for the uncovered edge for net loads ranging from 1.1 – 8.1 nN, showing that there is a substantial increase in the friction near the step edge for these loads. This contrasts the behavior at the covered edge, Fig. 2d, where we find that there is essentially no signature of a local increase in friction (estimated as a reduction of more than 90%). This result indicates graphene could be an ideal, atomically thin coating for reducing local friction associated with atomic steps.

The determination of the local topography from the LFM response is shown in Fig. 3 using both adhesion models (Eqs. (2) and (3)). Assuming a normally directed adhesion (Figs. 3a and 3b) erroneously suggests a topography over the graphene edge that is strongly dependent on L. In contrast, the vertically directed adhesion model results in a topography which is remarkably consistent over the same range of applied loads (Figs. 3c and 3d). This is a strong indication that the adhesion forces remain predominantly in the vertical direction as the tip traverses the atomic step edges. These topographic determinations also show excellent agreement with the simultaneously determined AFM height measurements for covered edges, uncovered edges, and regions of graphene that conform to the undulations of the substrate, as demonstrated by the agreement to the spatial derivative of the height measurements (black line) in Figs. 3c and 3d. Since the term $1 + \mu^2 \approx 1$ for low friction graphene surfaces, the AFM height measurements can be directly compared to the LFM Δ_{V_0} values to obtain the α calibration coefficient. This represents a new low-load LFM calibration method (compared to other techniques[33, 34]) that is sensitive to correct modeling of adhesion forces.

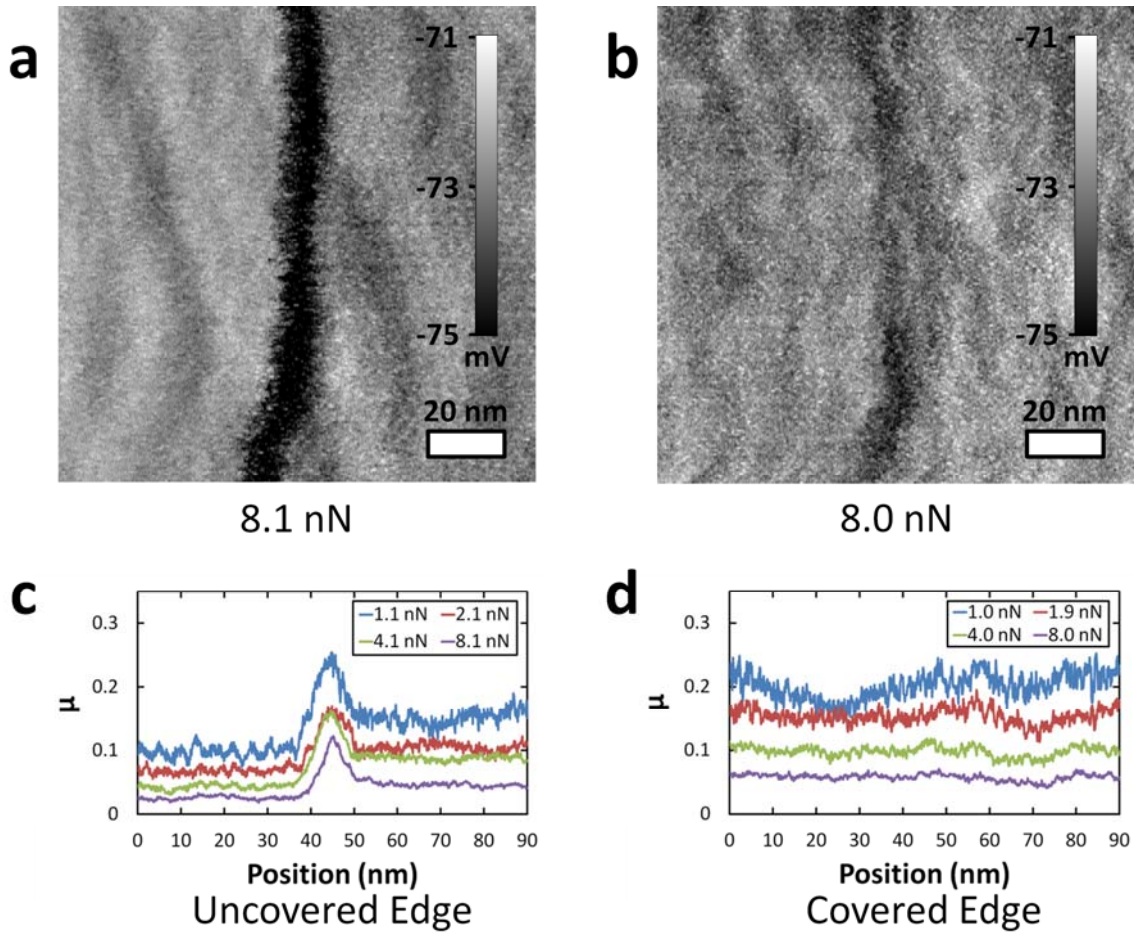

Figure 2: Local frictional characteristics of graphene edges: a-b, LFM retrace scans of an uncovered (**a**) and covered (**b**) graphene edge. For both scan regions the bi-layer graphene is on the left and the single layer is on the right. F_{net} for the scan in **a** is 8.1 nN with a 2.8 nN adhesion while the scan in **b** is 8.0 nN with a 2.6 nN adhesion. **c-d,** Analysis of line scan data from **a** and **b** at various loads using Eq. (1) in text. Data represent the average of 50 adjacent line scans over a width of 20 nm. The graphene edges correspond to a location in the middle of these plots (between 40 and 50 nm along the x-axis). The friction of the bi-layer region varies between **b** and **c** due to the change in scan angle (kept normal to the edge under investigation), which is consistent with recent reports of anisotropic frictional behavior of graphene surfaces.[23]

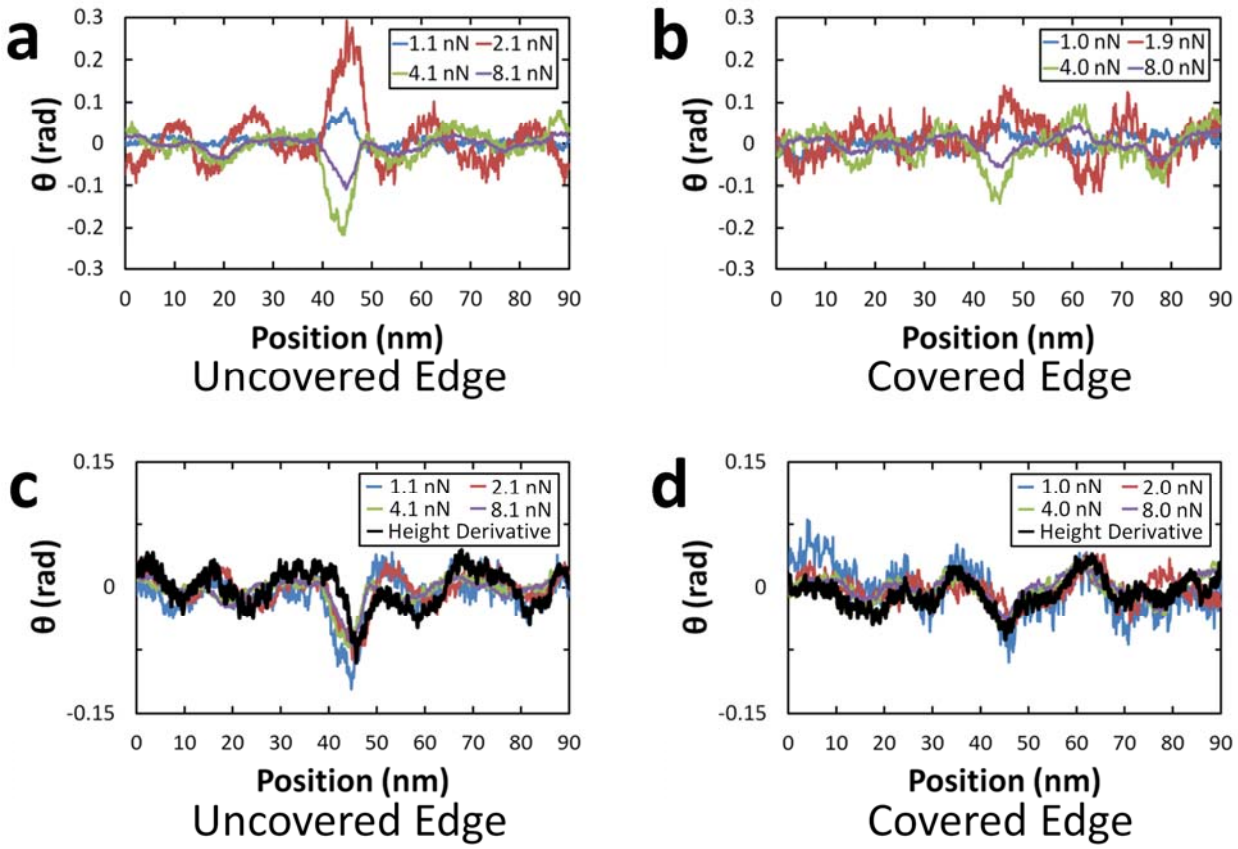

Figure 3: **Topography of graphene edges determined through LFM: a-b,** Analysis of line scan data from Fig. 2 at various loads using the normal adhesion model, Eq. (2) in text. **c-d,** Analysis of line scan data from Fig. 2 at various loads using the vertical adhesion model, Eq. (3) in text. The black line is the spatial derivative of the AFM height measurements. Data represent the average of 50 adjacent line scans over a width of 20 nm. The graphene edges correspond to a location in the middle of these plots (between 40 and 50 nm along the x-axis).

The above measurements were all performed with tips that were previously scanned laterally over regions of SiO_2 substrate resulting in tips with adhesions of 2.0 - 3.0 nN, a value consistent with previous reports.[25, 31] When we utilize tips that are scanned with low normal loads restricted only to the graphene regions, we observe lower adhesion forces of ~1.0 nN. These carefully maintained tips also show strongly altered LFM characteristics over exposed graphene edges. Figure 4a is a retrace scan of an exposed graphene edge, demonstrating an abrupt change in the lateral force as the tip moves up over the atomic step (going from a mono-layer to a bi-

layer region). A single line scan (Fig. 4b) reveals that as the tip is dragged into the graphene edge in the retrace direction, the LFM signal increases approximately linearly followed by an abrupt reduction in force at a location approximately 10 nm to the left. These LFM signals indicate that we are straining the exposed graphene edge as the tip moves up the step followed by a release of the stored elastic energy. These signals are repeatable over hundreds of trace/retrace cycles of the LFM tip (as in Fig. 4a) without noticeable displacement of the graphene edge, indicating that the edge is being elastically strained.

The effective spring constant, k, for flexing the graphene edge is estimated from the linear LFM response to be ~ 0.29 ± 0.11 N/m. This spring constant value of the graphene edge is nearly two orders of magnitude smaller than the torsional spring constant of the LFM tip $k_{tip} = GJ/(l(h + t/2)^2) \approx 24$ N/m,[33] where $G = 64$ Pa is the shear modulus of silicon, J is the torsion constant (approximated as $0.3wt^3$, where w is the $48\,\mu$m width and t is the $1\,\mu$m thickness of the cantilever), l is the $225\,\mu$m length of the cantilever, and h is the $12.5\,\mu$m height of the cantilever. Since $k \ll k_{tip}$, the vast majority of the deflection occurs within the graphene when the tip is laterally pressed against the graphene edge.

The stick-slip response of the graphene edge when laterally scanning with well-maintained, sharp tips can be qualitatively understood through extension of a recently proposed effective potential under low normal loads in the vicinity of an atomic step, $U = E\{-erf(x/b_1) + erf([x - c]/b_2)\}$.[29] In this model E is a constant of order an eV, b_1 is the effective barrier width at the edge ($x \equiv 0$) which should be on the order of the tip apex radius, and b_2 and c are constants larger than b_1 which represent a slow recovery of the potential. Assuming that such a potential describes the graphene edge, even when it has been flexed, the value of x represents the relative position of the tip to the graphene edge. Stick-slip motion of this relative coordinate as

the tip moves into the edge (in the $-\hat{x}$ direction) will occur at points where $\frac{d^2U}{dx^2} = -k$. Assuming reasonable values of $E = 2$ eV and $10b_1 = b_2 = c$ in the above potential with the observed spring constant of $k \approx 0.3$ N/m yields stick-slip behavior for $b_1 \lesssim 1$ nm. For atomic-scale effective barriers with $b_1 \approx 0.1$ nm the stick slip distance is ≈ 11 nm -- in good agreement with our experiments. As the effective tip apex and barrier width increase beyond 1 nm, the relative edge-tip distance is instead smoothly varying as the tip moves up the edge. This suggests that the smoothly varying lateral signal we observe for worn tips is due to their larger effective tip apex radii; a view also supported by their increased adhesion to the sample surface.

Covered edges do not show stick-slip flexing for the same well-maintained sharp tips and normal loads that cause this large ($\sim 10\,nm$) stick-slip flexing of uncovered edges. This suggests that a single covering layer of graphene increases the effective barrier width and/or decreases its depth to suppress stick-slip. The covering layer may also similarly act to suppress much smaller atomic-scale stick-slip displacements of the edge as a large-diameter worn tip (like the ones used to obtain the data in Figs. 1-3) moves over it. The reduction of atomic-scale stick-slip should likewise lead to the concomitant decrease in friction,[35] which could be the source of the significantly reduced friction observed for worn tips over covered edges in comparison to uncovered edges seen in Fig 2.

The energy stored in the large ($\sim 10\,nm$) uncovered graphene edge strain using well-maintained sharp tips is approximately $k(10\,nm)^2/2 \approx 90\,eV$. Estimates of possible in-plane strain energy are too large to account for this observed edge displacement. In-plane strain energy can be estimated with a two-dimensional model as $\frac{\pi L}{8}\frac{E}{1-\nu^2}x^2$ where E (≈ 1.02 TPa) is Young's modulus, L (≈ 0.34 nm) is the thickness of graphene, and ν (≈ 0.24) is the Poisson ratio for graphene[36] -- giving an energy of $9000\,eV$ for $x \approx 10$ nm displacement.[35]

In contrast, out-of-plane distortions (as represented in Fig. 4c) are much more consistent with our measurements. Although a detailed determination of possible out-of-plane strain energy is a subtle issue,[36] we obtain a rough estimate of it by considering the sum of the energy stored in bending a ~ 10 nm region of graphene in addition to the van der Waals (vdW) adhesion energy over this same region. The bending energy can be estimated through $2C \int dxdy(d^2u/dx^2)^2$, where u is the deflection and C (1.2 eV) is the bending stiffness.[37] Assuming a uniform bending radius of ~ 9 nm yields an energy of ~5 eV. An estimate of the adhesion energy over a ~ 10 nm diameter region can be estimated from the vdW adhesion energy (1.6×10^{18} eV/m^2)[37] to be ~130 eV. Since the sum of these out-of-plane energies is the same order of magnitude as our measurements, our observed edge strain is consistent with such a mode of deformation. Considering the large effects that such a strain can have on the transport properties of graphene,[12] the elastic response we observe represents a possible route for reversibly tuning the electronic properties of graphene.

It has also recently been suggested that out-of-plain elastic strain over the bulk portions of few-layer graphene samples could play an important role in the frictional dissipation for sharp asperities.[38] Likewise, the out-of-plane elastic strain indicated by our experiments could lead to additional modes of frictional energy dissipation at graphene edges.

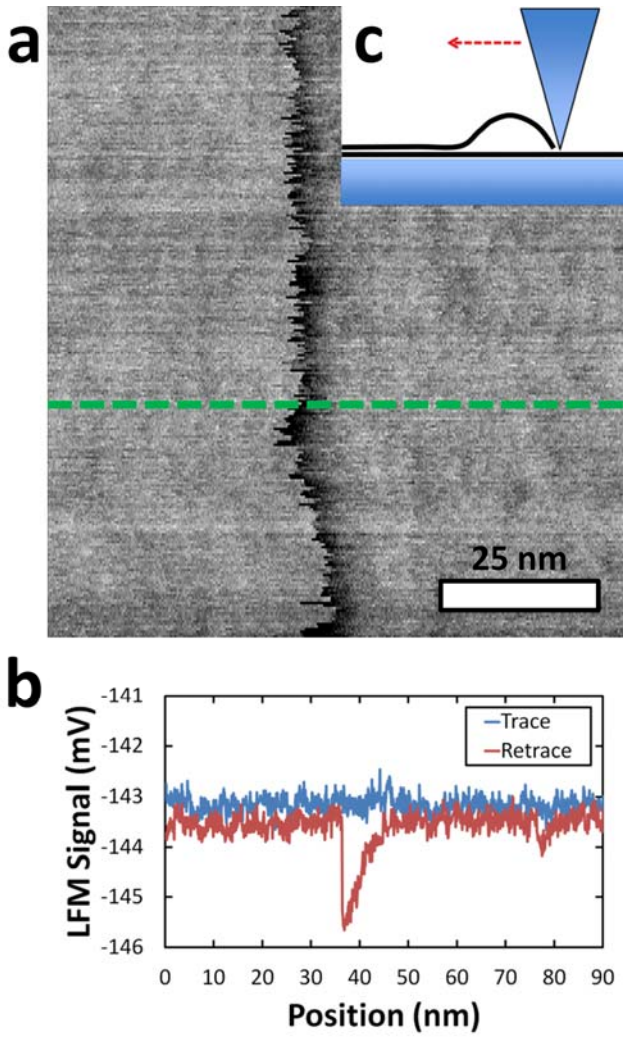

Figure 4: **Elastic response of graphene edge: a,** LFM retrace scan of a graphene edge. Bi-layer region is on the left, and single layer region is on the right. **b**, Single LFM scan lines in the trace and retrace directions as the tip is dragged across the edge. **c,** Schematic model of the tip causing out-of-plane strain of the edge as the tip is dragged towards it, to the right.

IV. CONCLUSIONS

We have observed frictional, adhesive, and elastic characteristics of graphene edges through the use of LFM. By focusing on single overlapping graphene layers (graphene crosses), LFM has revealed a significant local frictional increase at the exposed edges of graphene. In contrast, an edge covered by a single overlapping layer of graphene nearly completely removes this local frictional increase, indicating that graphene could be an ideal, atomically thin coating for

reducing local friction associated with atomic steps. Experimental comparison of LFM and AFM revealed that the local adhesion in the vicinity of graphene edges is directed vertically downwards. Taking this vertical adhesion into account allows for the surface topography of graphene to be determined through low-load LFM measurements and also provides a new low-load LFM calibration method. Through the use of low-adhesion scanning probe tips, we also observed evidence of elastic straining of graphene edges that act like nanoscale springs. Estimates of the strain energy are consistent with out-of-plane bending of graphene edges when atomically sharp LFM tips are dragged into them which causes a single large (~ 10 nm) stick-slip event. The elastic response we observe represents the reversible straining of graphene edges and could have application in future nanoscale electro-mechanical devices.

ACKNOWLEDGMENTS

The work was supported in part by the National Science Foundation (NSF) through Grant DMR-0805136, the Kentucky NSF EPSCoR program through award EPS-0814194, the University of Kentucky (UK) Center for Advanced Materials (CAM), and a Research Support Grant from the University of Kentucky Office of the Vice President for Research.

APPENDIX A: CANTILEVER AND SCANNING PROBE TIP CHARACTERIZATION

In order to apply precise load forces while scanning a sample, it is necessary to determine the spring constant (k) of a particular tip, as the actual value may vary significantly from the values supplied by the manufacturer. It is also necessary to determine the inverse optical lever sensitivity ($InvOLS$, units of nm/volt) which is the proportionality constant used to determine the deflection of the cantilever, in nanometers, from the vertical deflection voltage (V_{def}). From

these, we have $Z_{def} = InvOLS \cdot V_{def}$, and the applied load force $L = -k \cdot Z_{def}$, which when combined, allow us to apply a specific load force by setting V_{def}.

The net load force F_{net} (the average net force over a flat horizontal surface) is the sum of L and the adhesion force (A) between the tip and sample. In general, the adhesion force can depend on van der Waals (vdW) forces, sample charging, tip geometry, and environmental conditions such as humidity. Measurement of the adhesion force was done by bringing the tip into contact with the sample surface then retracting it while monitoring the deflection voltage to determine the force required to snap the tip off the sample surface (Fig. 5a). We found that differences in the tip-graphene and tip-SiO_2 adhesion forces are negligible for the results presented here (Fig. 5b). The adhesion force also tends to increase due to wear on the tip at high loads (Fig. 6) therefore the adhesion was measured between successive scans.

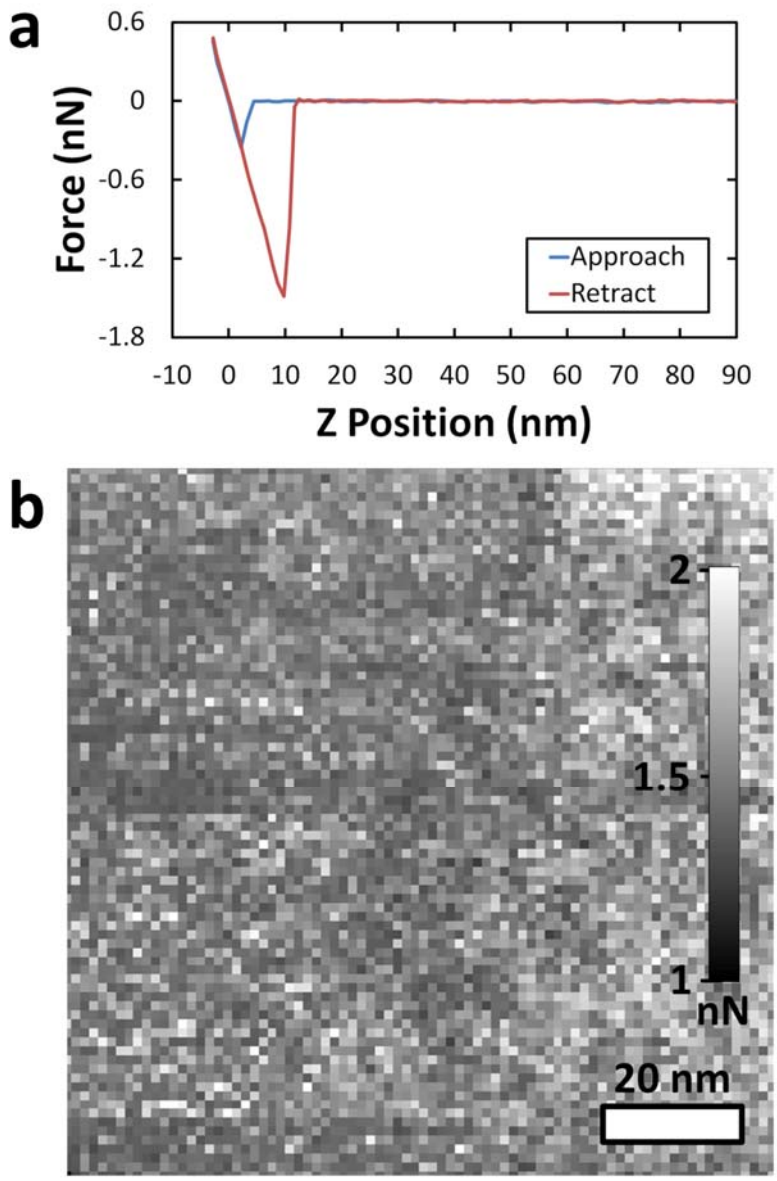

Figure 5: **Adhesion and force maps of sample: a,** The tip-sample adhesion force is measured by taking a force-distance curve. During this measurement, the tip is brought into hard contact with the sample surface. As the cantilever is retracted to withdraw the tip, adhesive forces oppose the release of the tip from the surface. The force measured just before the tip is released, in this case ≈1.5 nN, is the adhesion force. **b,** An adhesion force map is generated by taking a force-distance curve at every point during a scan centered about the same location as the AFM image, Fig. 1a, as shown above for a single-layer on single-layer graphene cross. On average, we find the differences in the tip-graphene and tip-SiO_2 adhesion forces to be less than 0.2 nN.

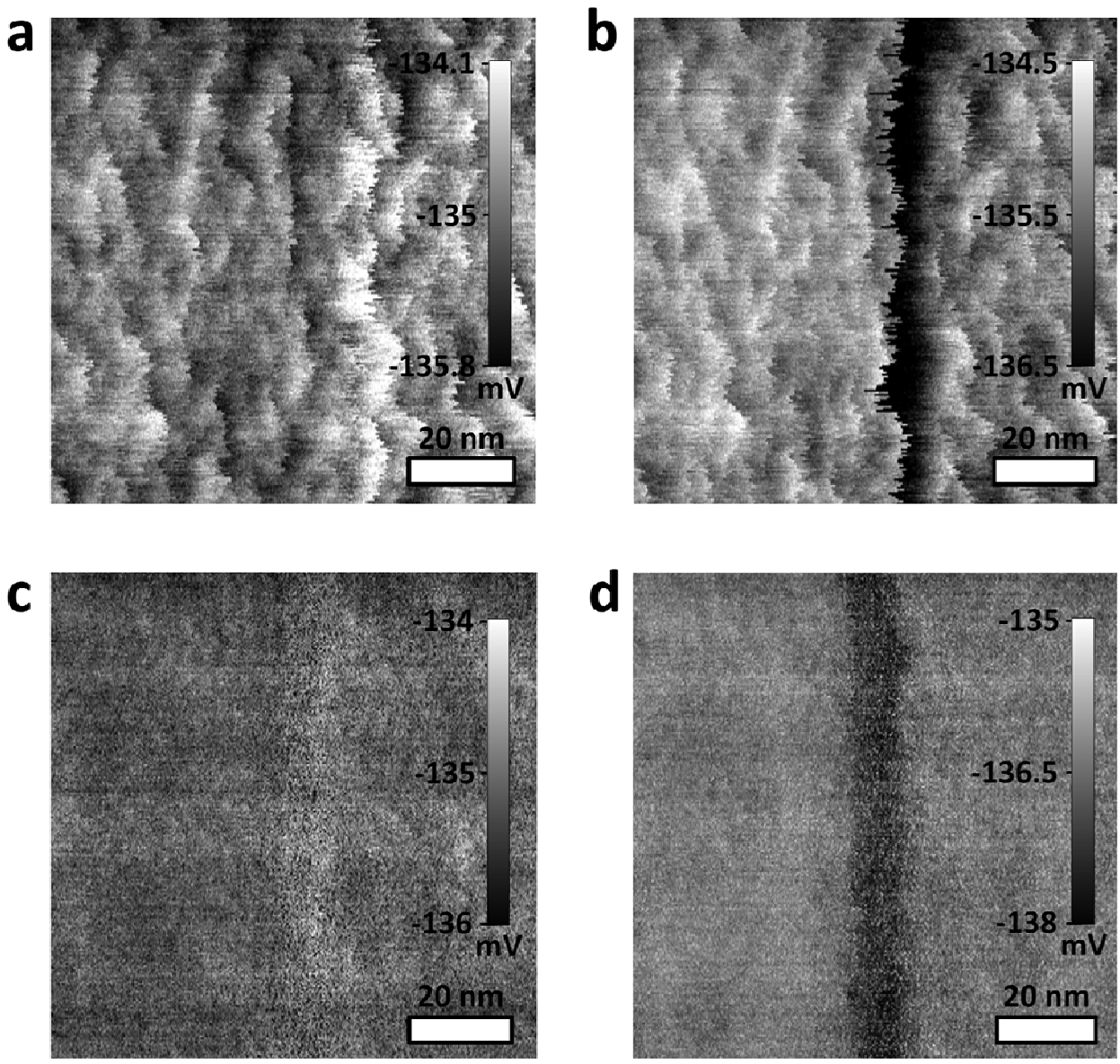

Figure 6: **Effects of tip-wear: a-b,** Trace and retrace LFM images, respectively, of an uncovered graphene step edge taken with a net applied load of 4.0 nN using a pristine LFM probe that exhibited an adhesion force of about ~1.0 nN. Note that the graphene edge compression features are enhanced. **c-d,** Respective LFM trace and retrace image comparisons of a similar region acquired with a net applied load of 3.9 nN with the same tip after it was scanned at a high load (approximately 20 nN) over the SiO_2 surface. The high-load scans were performed four times with a square window scan size of 125 nm and a scan rate of 0.6 Hz. The blunted tip exhibited an adhesion force of about 2.9 nN.

Crosstalk, the convolution of the lateral deflection voltages into the vertical deflection voltage channel and vice versa, must also be considered when making LFM measurements. This

crosstalk can have many possible sources, including a rotated PSD, asymmetries in the tip/cantilever, or large changes in either topographical or frictional features in the sample.[32] In these experiments, it was found that the degree of crosstalk was largely dependent on the tip being used and only probes that exhibited minimal crosstalk were used.

APPENDIX B: LATERAL FORCE MODELING

To quantify these changes in friction and morphology, we model the forces on an AFM cantilever tip as shown in the schematic in Figs. 1b and 1c as it is dragged over the local surface having an incline angle θ. The forces on the tip are balanced by the forces and moments applied to the AFM cantilever and will sum to zero assuming the tip is not accelerating. Separating the forces parallel and normal to the inclined surface yields respectively for the rightward (trace) motion of the tip,

$$T_t \cos\theta - L\sin\theta - F_{f_t} - A\sin\theta_A = 0 \tag{B1}$$

$$-T_t \sin\theta - L\cos\theta \mp N - A\cos\theta_A = 0, \tag{B2}$$

where the applied horizontal force on the cantilever is T_t, the vertical load applied to the cantilever is L, the frictional force at the tip is F_{f_t}, and A is the adhesion force on the tip which is directed at the angle of θ_A with respect to the normal of the surface. We will also assume Amonton's law such that $F_{f_t} = \mu N$, where μ is the coefficient of friction and N is the normal force acting on the tip from the surface. This normal force can be eliminated from equations (B1) and (B2) and solved for T_t such that

$$T_t = \frac{L(\sin\theta + \mu\cos\theta) + A(\sin\theta_A + \mu\cos\theta_A)}{\cos\theta - \mu\sin\theta}. \tag{B3}$$

We will assume small angles for the topography so that θ and θ_A are small and we can approximate T_t as

$$T_t \approx \frac{L(\theta+\mu)+A(\theta_A+\mu)}{1-\mu\theta}. \quad \text{(B4)}$$

Likewise, the horizontal force for the leftward (retrace) motion of the tip is

$$T_r = \frac{L(\sin\theta-\mu\cos\theta)+A(\sin\theta_A-\mu\cos\theta_A)}{\cos\theta+\mu\sin\theta} \approx \frac{L(\theta-\mu)+A(\theta_A-\mu)}{1+\mu\theta}. \quad \text{(B5)}$$

Assuming a small tilt angle φ for the cantilever and requiring that the sum of the moments about the tip of the cantilever be zero we obtain

$$M_t - \left(h+\frac{t}{2}\right)T_t - L\left(h+\frac{t}{2}\right)\varphi_t = 0, \quad \text{(B6)}$$

where M_t is the constraining moment applied by the fixed base of the cantilever, h is the AFM tip height, and t is the cantilever beam thickness. Since the externally applied moment is in response to the torsional rotation of the cantilever by φ, we can relate the two quantities through

$$\varphi_t = \frac{M_t l}{GJ}, \quad \text{(B7)}$$

where l is the length of the cantilever, G is the shear modulus, and J is the torsion constant of the cantilever which depends on its geometrical cross section. Equation (B6) can now be written as

$$M_t\left\{1-\frac{L\left(h+\frac{t}{2}\right)l}{GJ}\right\} = \left(h+\frac{t}{2}\right)T_t. \quad \text{(B8)}$$

For the cantilevers we use and for vertical cantilever loads $L \lesssim 10\ nN$, we have $\frac{L\left(h+\frac{t}{2}\right)l}{GJ} \ll 1$, so that Eq. (B8) can be approximated as

$$M_t = \left(h+\frac{t}{2}\right)T_t, \quad \text{(B9)}$$

with a similar relation for the retrace scan direction.

In LFM, we measure a voltage signal for the trace direction V_t that is related to the torsional rotation and, thus, the torsional moment on the cantilever. For small torsional angles this relation is (for both trace and retrace signals respectively)

$$V_t = V_0 + \frac{M_t}{\alpha\left(h+\frac{t}{2}\right)}, \tag{B10}$$

and

$$V_r = V_0 + \frac{M_r}{\alpha\left(h+\frac{t}{2}\right)}, \tag{B11}$$

where V_0 is an offset and α is the LFM calibration coefficient where the term $\alpha\left(h+\frac{t}{2}\right)$ converts a torsional moment applied to the cantilever to the measured voltage. For a flat surface with the lateral force only due to frictional effects, the term $\frac{M_t}{\left(h+\frac{t}{2}\right)}$ is the frictional force. We can determine the local frictional and topographical changes using the above relations by taking half the difference ($\mathrm{W}_V = (V_t - V_r)/2$) and the average ($\Delta_V = (V_t + V_r)/2$,) of the trace and retrace voltage measurements, such that

$$\mathrm{W}_V = \frac{1}{2\alpha}(T_t - T_r) \approx \frac{\mu(L+A)}{\alpha}, \tag{B12}$$

and,

$$\Delta_{V\,0} = \Delta_V - V_0 = \frac{1}{2\alpha}(T_t + T_r) \approx \frac{L\theta + A\theta_A + (L+A)\mu^2\theta}{\alpha}, \tag{B13}$$

where we have only kept terms to linear order in the small angles. The V_0 baseline can be estimated by taking the spatial average of Δ_V over a region where we expect θ and θ_A to vary equally on either side of zero. We use the flat regions over uniform thicknesses of FLG to perform this baseline determination.

Equation (B12) can be inverted to determine the local coefficient of friction from experimentally determined values such that,

$$\mu = \frac{\alpha \mathrm{W}_V}{(L+A)}. \tag{B14}$$

The local coefficient of friction of a surface can be obtained once the calibration coefficient α is determined.

Unlike the coefficient of friction, the local topography determined by the measurements is highly influenced by the relation between θ and θ_A. Conventionally, θ_A is chosen to be zero such that the adhesion is always directed normal to the local contact between the AFM tip and the surface. However, this choice is not necessarily valid for very short inclines that are appropriate for atomic scale changes in topography. Thus we arrive at the two possible cases: For normal adhesion we have,

$$\theta = \frac{\alpha \Delta_{V_0}}{L+(L+A)\mu^2}, \tag{B15}$$

while for vertical adhesion we have,

$$\theta = \frac{\alpha \Delta_{V_0}}{(L+A)(1+\mu^2)}. \tag{B16}$$

For both cases we consider here for the adhesion, the local coefficient of friction can be determined from Eq. (B14) and inserted into Eqs. (B15) and (B16) to determine the local slope of the topography.

REFERENCES

1 A. K. Geim and K. S. Novoselov, Nature Materials **6**, 183 (2007).
2 K. S. Novoselov, A. K. Geim, S. V. Morozov, D. Jiang, Y. Zhang, S. V. Dubonos, I. V. Grigorieva, and A. A. Firsov, Science **306**, 666 (2004).
3 C. Berger, et al., Journal of Physical Chemistry B **108**, 19912 (2004).
4 K. I. Bolotin, K. J. Sikes, Z. Jiang, M. Klima, G. Fudenberg, J. Hone, P. Kim, and H. L. Stormer, Solid State Communications **146**, 351 (2008).
5 S. Dutta and S. K. Pati, J. Mater. Chem. **20**, 8207 (2010).
6 X. Jia, J. Campos-Delgado, M. Terrones, V. Meunier, and M. S. Dresselhaus, Nanoscale **3**, 86 (2011).
7 X. Jia, et al., Science **323**, 1701 (2009).
8 C. O. Girit, et al., Science **323**, 1705 (2009).
9 S. S. Datta, D. R. Strachan, S. M. Khamis, and A. T. Johnson, Nano Lett. **8**, 1912 (2008).
10 Y. Lu, B. Goldsmith, D. R. Strachan, J. H. Lim, Z. Luo, and A. T. C. Johnson, Small **6**, 2748 (2010).
11 F. Guinea, M. I. Katsnelson, and A. K. Geim, Nature Physics **6**, 30 (2010).
12 N. Levy, S. A. Burke, K. L. Meaker, M. Panlasigui, A. Zettl, F. Guinea, A. H. C. Neto, and M. F. Crommie, Science **329**, 544 (2010).

[13] F. de Juan, A. Cortijo, M. A. H. Vozmediano, and A. Cano, Nature Physics **7**, 810 (2011).
[14] F. Guinea, M. I. Katsnelson, and M. A. H. Vozmediano, Physical Review B **77**, 075422 (2008).
[15] F. Guinea, B. Horovitz, and P. Le Doussal, Physical Review B **77** (2008).
[16] V. B. Shenoy, C. D. Reddy, A. Ramasubramaniam, and Y. W. Zhang, Physical Review Letters **101**, 245501 (2008).
[17] A. Cresti, M. M. Fogler, F. Guinea, A. H. C. Neto, and S. Roche, Physical Review Letters **108**, 166602 (2012).
[18] F. Guinea, A. K. Geim, M. I. Katsnelson, and K. S. Novoselov, Physical Review B **81**, 035408 (2010).
[19] M. M. Fogler, A. H. Castro Neto, and F. Guinea, Physical Review B **81**, 161408 (2010).
[20] E. Prada, P. San-Jose, G. Leon, M. M. Fogler, and F. Guinea, Physical Review B **81**, 161402 (2010).
[21] C. Lee, X. D. Wei, J. W. Kysar, and J. Hone, Science **321**, 385 (2008).
[22] T. Filleter, J. L. McChesney, A. Bostwick, E. Rotenberg, K. V. Emtsev, T. Seyller, K. Horn, and R. Bennewitz, Physical Review Letters **102**, 086102 (2009).
[23] C. Lee, Q. Y. Li, W. Kalb, X. Z. Liu, H. Berger, R. W. Carpick, and J. Hone, Science **328**, 76 (2010).
[24] H. Lee, N. Lee, Y. Seo, J. Eom, and S. Lee, Nanotechnology **20**, 325701 (2009).
[25] J. S. Choi, et al., Science **333**, 607 (2011).
[26] C. M. Mate, G. M. McClelland, R. Erlandsson, and S. Chiang, Physical Review Letters **59**, 1942 (1987).
[27] D. R. Baselt and J. D. Baldeschwieler, Journal of Vacuum Science & Technology B **10**, 2316 (1992).
[28] G. Meyer and N. M. Amer, Appl. Phys. Lett. **57**, 2089 (1990).
[29] P. Steiner, E. Gnecco, F. Krok, J. Budzioch, L. Walczak, J. Konior, M. Szymonski, and E. Meyer, Physical Review Letters **106**, 186104 (2011).
[30] H. Holscher, D. Ebeling, and U. D. Schwarz, Physical Review Letters **101**, 246105 (2008).
[31] T. Muller, M. Lohrmann, T. Kasser, O. Marti, J. Mlynek, and G. Krausch, Physical Review Letters **79**, 5066 (1997).
[32] M. W. Such, D. E. Kramer, and M. C. Hersam, Ultramicroscopy **99**, 189 (2004).
[33] M. Varenberg, I. Etsion, and G. Halperin, Rev. Sci. Instrum. **74**, 3362 (2003).
[34] D. F. Ogletree, R. W. Carpick, and M. Salmeron, Review of Scientific Instruments **67**, 3298 (1996).
[35] V. L. Popov, *Contact Mechanics and Friction, Physical Principles and Applications* (Springer-Verlag, Berlin Heidelberg, 2010).
[36] D. B. Zhang, E. Akatyeva, and T. Dumitrica, Physical Review Letters **106**, 255503 (2011).
[37] S. Cranford, D. Sen, and M. J. Buehler, Applied Physics Letters **95**, 123121 (2009).
[38] A. Smolyanitsky, J. P. Killgore, and V. K. Tewary, Physical Review B **85** (2012).